Enhancing Multiplicity Analysis with a Position-Corrected Efficiency Algorithm through List-Mode data acquisition

Authors: Cole J. Thompson, Robert Weinmann-Smith, Brian Weaver, Nik Economy, Martyn Swinhoe, Vlad Henzl, Marc Ruch, Audrey Roman, Duc Vo, Rollin Lakis

Affiliation: Los Alamos National Laboratory, P.O. Box 1663, Los Alamos, NM, 87545

1. INTRODUCTION

Waste assay is a process to characterize the amount of nuclear material contained within a matrix or media that is no longer of valuable use to the project or process. The physical, chemical, and isotopic information associated with the amount of nuclear material are also often of interest for long-term storage requirements. Destructive analysis (DA) methods can provide the requisite information for waste assay with high accuracy and low uncertainty for homogenous samples, but their cost and measurement time can be prohibitive. Nondestructive assay (NDA) is an alternative to DA, but there are still tradeoffs between cost, measurement time, and uncertainty. Calorimetry is the gold standard NDA technique for quantification of nuclear material for both accuracy and uncertainty but requires both additional isotopic information and measurement times up to twenty-four hours, which, like DA, can be prohibitive. An alternative to calorimetry is the combination of gamma-ray spectroscopy for isotopic identification and neutron counting for nuclear material quantification. This method provides a result with a larger uncertainty than DA or calorimetry but can be performed on a timescale of minutes instead of hours or days.

For neutron NDA there are three unknown variables of interest: alpha (α) (ratio of (α, n) neutrons to spontaneous fission neutrons), multiplication (*M*), and effective ^{240}Pu mass ($^{240}Pu_{eff}$) [1]. To determine these unknowns, three equations are needed [2]. These equations come from the neutron point model,

$$\text{Singles} = m * F * \varepsilon * \nu_{s1} * M_L * (1 + \alpha) \tag{1}$$

$$\text{Doubles} = m * F * \frac{\varepsilon^2}{2} * f_d * {M_L}^2 * \left[\nu_{s2} + \frac{(M_L - 1)}{(\nu_{i1} - 1)} * \nu_{s1} * \nu_{i2} * (1 + \alpha)\right] \tag{2}$$

$$\text{Triples} = m * F * \frac{\varepsilon^3}{6} * f_t * {M_L}^3 \left[\nu_{s3} + \frac{(M_L - 1)}{(\nu_{i1} - 1)}[3\nu_{s2}\nu_{i2} + \nu_{s1}(1 + \alpha)\nu_{i3}] + 3\left[\frac{(M_L - 1)}{(\nu_{i1} - 1)}\right]^2 * \nu_{s1} * {\nu_{i2}}^2\right] \tag{3}$$

where *F* is the fission rate, ε is the instrument efficiency, *M* is the neutron leakage multiplication, α is the ratio of (α, n) reactions to spontaneous fissions, f_d is the doubles gate fraction, and f_t is the triples gate fraction. There are methods where not all equations are needed, such as the calibration curve approach and known-alpha method. However, if assumptions for these approaches cannot be held reliable or assay flexibility is important, then neutron multiplicity counting can be used. This method is based on the mathematical model underlying Eq. (1), Eq. (2), and Eq. (3) to solve for all three unknowns. While each of these methods has different assumptions and requires a varying amount of data, they are all tied together by a central thread: instrument efficiency. The instrument efficiency and its associated uncertainty are implicitly included in a calibration curve and the known-alpha method or included as a variable that needs uncertainty propagation in neutron multiplicity counting.

For an instrument performing waste NDA there are many sources of uncertainty that contribute to the total measurement uncertainty (TMU). The uncertainty of the efficiency, which is a function of radial and axial position, can be the largest single contributor. Historically, this uncertainty has been abstracted into the uncertainty related to matrix identity and source distribution, both of which impact neutron scattering and, therefore, instrument response. This is the case for other waste NDA instruments like the High Efficiency Passive Neutron Counter (HENC), where matrix identity uncertainty is 12% and source distribution

uncertainty ranges from 5-22% depending on the waste, and the Waste Drum Assay System (WDAS) [3, 4]. To help account for these sources of uncertainty, HENC and WDAS both use the Add-a-Source method to perform a volume-averaged correction for the matrix material to the measured doubles rate. However, the Add-a-Source method does not perform a correction for source position or distribution.

This work presents an algorithm using list-mode data readout and modified ^{3}He tube lengths to decrease the uncertainty associated with efficiency as a function of position. The benefits of doing so are two-fold:

1. A lower instrument TMU, which allows for more waste to be packed into a waste drum within the bounds of regulatory constraints.
2. A decrease in total waste drums because waste drums can be filled more completely. This helps extend the lifetime of waste repositories, like the Waste Isolation Pilot Plant—the United States' long-lived radioactive waste repository for disposal of defense-generated waste [5].

As a proof-of-concept this position-corrected efficiency (PCE) algorithm is used to augment neutron multiplicity analysis using MCNP simulated data of a plutonium source in the High-Level Neutron Counter with list-mode data readout capabilities (HLNC-LM) [6]. This algorithm is one specific example of list-mode data readouts improving neutron NDA, but there are many additional potential applications.

This work first outlines the standard method used to determine instrument efficiency and its associated uncertainty. Then the hardware, software, and data acquisition electronics that enable this capability are briefly described. A detailed description of the physical structure and data-processing steps for the PCE algorithm follow. Then MCNP simulations are described and the data from these MCNP simulations are used to perform multiplicity analysis in two ways:

1. Using the **standard method** of determining the efficiency of a detector and its associated uncertainty.
2. Using the **position-corrected efficiency algorithm,** which has axial and radial resolution, to update the efficiency value and its associated uncertainty.

Different forms of the PCE algorithm described in this work are available, specifically with only radial resolution, but are not presented here. Benchmarking the PCE algorithm to measured data from the HLNC-LM with only radial resolution and to an instrument with axial and radial resolution is left for future work.

2. LIST-MODE DATA ACQUISITION CAPABILITIES AND SYSTEM

List-mode data has existed for radiation and physics measurements for many decades. The advances enabling this algorithm represent the culmination of approximately ten years of development and provide great potential to advance neutron NDA and other research areas, including:

- KM-200 preamplifier modules that enable advanced analysis at the preamplifier signal level [7].
- The Advanced List-Mode Module (ALMM) which replaces the shift register in neutron NDA [8].
- INCC6, which can collect list-mode data with data acquisition software (like the ALMM) [9].
- Neutron counters, like the HLNC-LM, designed to take advantage of list-mode capabilities.
- Analysis methods, like the one described in this work, to take advantage of list-mode data.

2.1 HLNC-LM

The HLNC-LM is an updated version of the HLNC with list-mode data readout capabilities [10]. There are eighteen ^{3}He tubes each with an active length of 20 in. (50.8 cm) and fitted with a KM200 preamplifier. The data from the preamplifiers are sent via ribbon cable to the ALMM. INCC6 can read the ALMM output file to provide the singles rate for each of the eighteen ^{3}He tubes and the coincidence matrix. The traditional shift register output of singles, doubles, and triples rates is also reported. The HLNC-LM well height is 16 in. (40.64 cm) with a diameter of 6.70 in. (17.018 cm). Side and top views of the MCNP geometry of the HLNC-LM are shown in Figure 1.

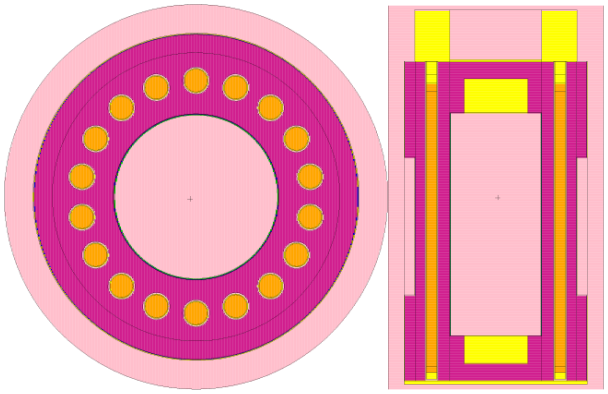

Figure 1. Top-down and side views from MCNP6.2 of the HLNC-LM.

3. VOLUME-AVERAGE EFFICIENCY

The volume-average efficiency is a weighted average of efficiency values at many points in the instrument well. For this approach, the efficiency values are taken at the vertices of a voxel and averaged together to give each voxel an efficiency value. The weight given to each voxel is proportional to the fraction of total volume contained within the voxel. This work uses fifteen data points in a grid of three radial positions at five different axial positions. Figure 2 provides a two-dimensional example of this approach and the weights given to an area (or a slice through a voxel).

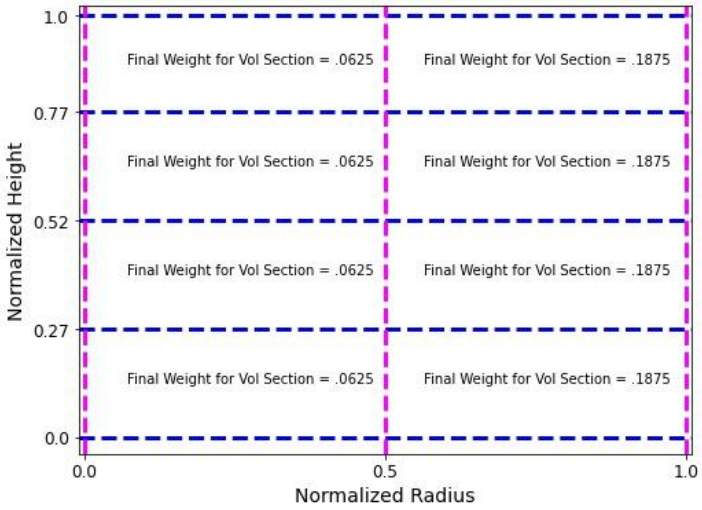

Figure 2. Visualization of the three radii and five heights sampled and the weight assigned to each voxel in the volume-average efficiency calculation.

The volume-average efficiency can be calculated for different matrix materials filling the instrument well, as each matrix has different neutron interaction rates based on isotopic composition and density. More importantly, the volume-average efficiency is an approach to summarize efficiency variance as a function of radius and height as a single value. However, the efficiency in the instrument well changes as a function of both radius and height. Figure 3 shows the change in MCNP-simulated efficiency as a function of height (left) and as a function of radius (right) for the HLNC-LM well when filled with air.

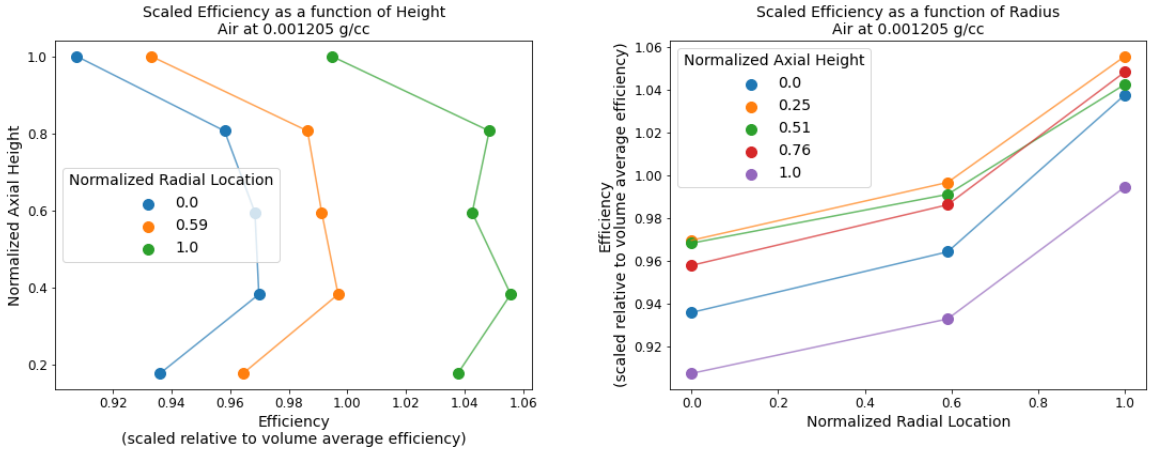

Figure 3. Profiles of the efficiency in the HLNC-LM instrument well. Left: Efficiency as a function of height. Right: Efficiency as a function of radius.

As a result of calculating a single volume-average efficiency in the standard approach, the assayed $^{240}Pu_{eff}$ for a small point-like source is ***not*** invariant to changes in efficiency as a function of height or radius, leading to large deviations in the assayed $^{240}Pu_{eff}$ compared to declared $^{240}Pu_{eff}$, as shown in Figure 4. However, when assaying waste cans or drums, the sampling efficiency for the volume of waste in the instrument well is averaged across the distributions shown in Figure 4, which reduces to the volume-average efficiency when the instrument well is entirely filled.

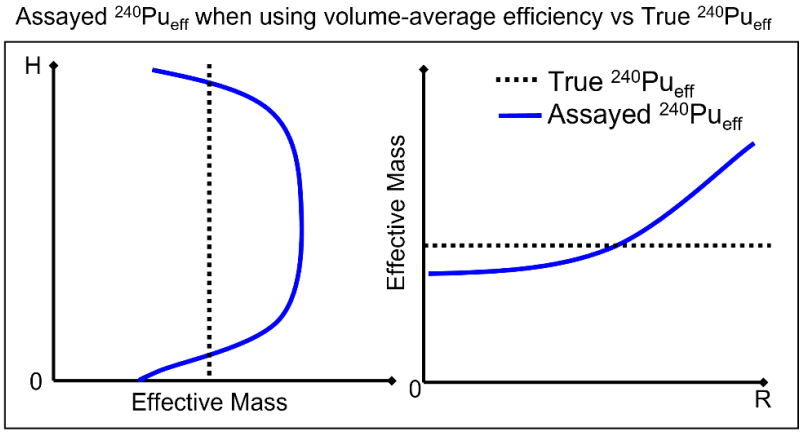

Figure 4. Visual representation of how assayed $^{240}Pu_{eff}$ changes as a function of height and radius in an instrument well using the volume-average efficiency.

4. POSITION-CORRECTED EFFICIENCY (PCE) ALGORITHM

The PCE algorithm updates the efficiency term used in multiplicity analyses. This allows the assayed $^{240}Pu_{eff}$ to be calculated using an efficiency value that is closer to the true value for a given height and radius, which decreases the instrument TMU. The PCE algorithm does this by using both radial and axial resolution. Axial resolution is created by modifying the heights of a group of ^{3}He tubes, called a bank, such that there are three heights: full-length (shown in blue in Figure 5), long (shown in green in Figure 5), and short (shown in pink in Figure 5). The long tubes are five-sixths and short tubes are one-sixth the height of the full-length tube. Short tubes are more sensitive to the signal near the bottom of the instrument well, long tubes are more sensitive to the signal near the top of the instrument well, and full-length tubes are invariant to axial position in the instrument well. There are four axial banks used in the HLNC-LM to improve the detection efficiency across the instrument well and to decrease sensitivity of the signal to source location. As before, all ^{3}He tubes regardless of height are fitted with their own KM200 preamplifier.

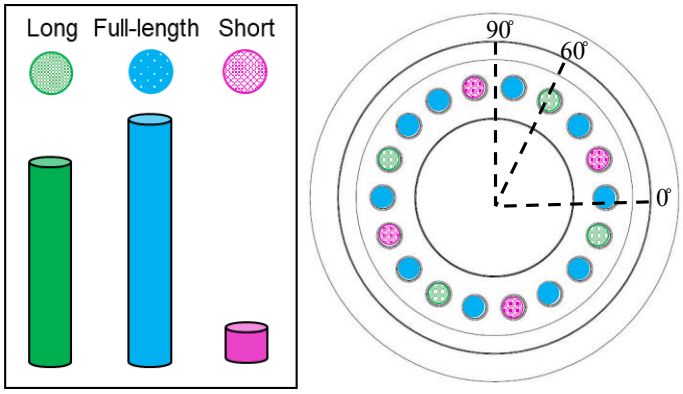

Figure 5. Physical layout of the PCE algorithm for HLNC-LM. The angular planes used in simulation are also denoted.

The individual readout data from the HLNC-LM modified for the PCE algorithm are combined in specific ways to create an axial and radial statistic. These statistics translate count-rate data into a measure of the effective axial or radial position of the assayed item. The functional forms for calculating each statistic were selected because they returned the best fits from all equations tried. The axial statistic combines the data from each of the three tubes in an axial bank together, following Eq. (4):

$$Q_{axial} = \ln\left(\frac{\sum_{i=1}^{N} Q_{bank}(i)}{N}\right) \qquad Q_{bank}(i) = \frac{\sqrt{S_{short}(i)} * \sqrt{S_{long}(i)}}{\left(S_{full}(i)\right)} \tag{4}$$

This value is calculated for each axial bank, *i*, and the average of the values across all axial banks is the final value of the axial statistic. In these analyses, the HLNC-LM is modified to have four axial banks. During calibration, the radial statistic is calculated using only the full-length tubes (shown in blue in Figure 5) according to Eq. (5):

$$Q_{radial} = \frac{{S_{min}}^{0.5}}{{S_{max}}^{1.5}} \tag{5}$$

During operational use, the radial statistic must use a scaling factor from the calibration measurements to account for changes in source strength according to Eq. (6):

$$Q_{radial} = \frac{{S_{min}}^{0.5}}{{S_{max}}^{1.5}} * \frac{(S_{max}/\text{Calibration}_{max})^{1.5}}{(S_{min}/\text{Calibration}_{min})^{0.5}} \tag{6}$$

5. POSITION-CORRECTED EFFICIENCY (PCE) ALGORITHM STEPS

5.1 Calibration

The data needed for the calibration steps of the PCE algorithm include:

1. Data from each ^{3}He tube for positions spanning radial, angular, and axial positions in the instrument well in accordance with the volume-averaged efficiency algorithm. These positions need to be assayed for each combination of matrix material and matrix material density of interest. Simulated data, while rarely used for deployed instruments, can be used (as done for this work).
2. Volume-average efficiency values and associated one sigma standard deviation for each combination of matrix material and matrix material density of interest.

These data are used to calibrate the PCE algorithm as follows:

1. Data from different radial, angular, and axial positions for combinations of matrix material and matrix material density of interest are processed.
    a. Axial positions are converted into normalized values between zero and one, where zero corresponds to the bottom of the instrument well in terms of height and one corresponds to the top of the instrument

well in terms of height. In practical application, zero will correspond to the centroid of the source used when placed at the bottom of the instrument well and one will correspond to the centroid of the source when placed as high as possible in the instrument well.

b. Radial positions are converted into normalized values between zero and one, where zero corresponds to the center of the instrument well radially and one corresponds to the furthest edge of the instrument well radially. In practical application one will correspond to the centroid of the source when placed as far to the outside of the instrument well as physically possible.

c. The singles rate efficiency at each position is calculated and then scaled by the volume-average efficiency for that combination of matrix material and matrix material density.

2. The data from axial banks for all positions of a specific combination of matrix material and matrix material density are processed to create a curve that relates the axial statistic to a normalized axial value.

a. For each position, an axial statistic is calculated using Eq. (4) (above).

b. The logarithm of the axial statistic for each position is plotted against the normalized axial value of that position, and the polynomial functional form outlined in Eq. (7) is fit for each matrix material and matrix material density. The coefficients of best fit are saved for operational use. The functional form of Eq. (7) was selected as it returned the best fit of all equations tested.

$$\text{Normalized Axial Value} = \left(A * \ Q_{axial}{}^2\right) + (B * \ Q_{axial}) + C \tag{7}$$

3. The data for all full-length tubes for all positions of a specific combination of matrix material and matrix material density are processed to create a curve that relates the radial statistic to a normalized radius value.

a. For each position, a radial statistic is calculated using Eq. (5) (above).

b. The radial statistic for each position is plotted against the normalized radial value of that position, and the logarithmic functional form outlined in Eq. (8) is fit for each matrix material and matrix material density. The coefficients of best fit are saved for operational use. The functional form of Eq. (8) was selected as it returned the best fit of all equations tested.

$$\text{Normalized Radial Value} = (A * \ln(Q_{radial})) + b \tag{8}$$

4. A multiple linear regression is fit to all the data points for a specific combination of matrix material and matrix material density to predict the scaled singles efficiency (SSE), which is the singles rate efficiency at each position divided by the volume-average efficiency. The predicted SSE is then used in multiplicity analysis. Four input variables are used in the regression to predict the SSE: normalized radial value, normalized axial value, the square of the normalized radial value, and the square of the normalized axial value. The squared terms are necessary for best performance because the efficiency curves in both the radial and axial directions are second-order polynomials, as shown in Figure 3.

a. All calculated SSE values and corresponding normalized radial and axial values are used to fit Eq. (9).

$$\widehat{\text{Scaled Singles}}\ \text{Efficiency} = \beta_0 + (\beta_1 * r_{normalized}) + (\beta_2 * r_{normalized}{}^2) + (\beta_3 * ax_{normalized}) + (\beta_4 * ax_{normalized}{}^2) \tag{9}$$

b. The coefficients of best fit for each variable and the intercept are saved for operational use.

c. The relative root mean square error (RRMSE), defined in Eq. (10), of the linear regression fit to the ground truth data is saved for use as the one sigma value for uncertainty on any predicted value during operational use. The RRMSE captures the variance in the residuals associated with the multiple linear regression model.

$$\text{RRMSE} = 100 * \sqrt{\sum_{i=0}^{N} \frac{\left(\left(Y_i - \hat{Y}_i\right)/Y_i\right)^2}{N}} \tag{10}$$

5.2 Operation

The data needed for operational use of the PCE algorithm include:

1. Data at radial, angular, and axial positions of interest for a specific combination of matrix material and matrix material density. For best performance, matrix material and matrix material density should be known.

These data are then used in the operation mode of the PCE algorithm as follows:

1. The data for axial banks are processed to calculate the axial statistic which is then used to predict a normalized axial value.
   a. The axial statistic is calculated using Eq. (4).
   b. The coefficients of the axial polynomial fit for the specific matrix material and matrix material density are loaded into the functional form defined in Eq. (7).
   c. The axial polynomial fit is evaluated using the natural logarithm of the axial statistic as the input variable. This outputs a prediction for normalized axial value. Values of the axial statistic are clipped to be between zero and one.
2. The data for all full-length tubes are processed to calculate the radial statistic that is then used to predict a normalized radius value.
   a. The radial statistic is calculated using Eq. (6). This is because the coefficients for which the radial logarithmic function were fit during calibration are specific to the source strength at that step.
   b. The coefficients for the radial logarithmic fit for that specific matrix material and matrix material density are loaded into the functional form defined in Eq. (8).
   c. The radial logarithmic fit function is evaluated using the radial statistic value as the input variable. This outputs a prediction for normalized radial value.
3. The predicted normalized radial value and the predicted normalized axial value are used in the linear regression function to predict the SSE of the current position.
   a. The coefficients of the linear regression fit for the specific matrix material and matrix material density are loaded into the functional form described in Eq. (9).
   b. The linear regression fit is evaluated with the following four inputs to predict a scaled single efficiency term:
      i. Predicted normalized radial value
      ii. The square of the predicted normalized radial value
      iii. Predicted normalized axial value
      iv. The square of the predicted normalized axial value
   c. The predicted SSE term is multiplied by the volume-average efficiency to update the raw singles efficiency term. The RRMSE is multiplied by the updated raw singles efficiency term to determine the one sigma uncertainty of the updated raw singles efficiency value.
   d. The updated raw singles efficiency value and the associated one sigma uncertainty are used in the multiplicity equations as a replacement for the volume-average efficiency and its uncertainty.

6. SIMULATION DESCRIPTION

MCNP6.2 simulations of a metal plutonium source, with isotopics listed in Table IA, were performed at fifteen locations within the HLNC-LM. These correspond to the radial and height locations shown in Figure 2. These simulations were conducted at three different angular planes, 0, 60, and 90 degrees, as shown in Figure 5, inside the instrument well for the thirty-one combinations of matrix and matrix density outlined in Table IB. At each of the fifteen locations, two sets of simulations were performed. The first set treated ^{3}He tubes normally, i.e., using a single defined active volume for each ^{3}He tube. For this set of simulations, F4 Volume Averaged Flux Tallies and F8 Pulse Height Tallies were performed for each individual tube and for

all eighteen ^{3}He tubes. The second set of simulations split the active volume of each ^{3}He tube into six sections to create axial resolution. F4 Volume Averaged Flux tallies were performed for each of the six sections of active volume for each of the eighteen ^{3}He tubes. All simulations were run with 1E8 histories.

Table IA. Pu Source Isotopics

Isotope	Mass Percent (%)
^{238}Pu	1.18E–2
^{239}Pu	93.8122
^{240}Pu	5.9304
^{241}Pu	5.19E–2
^{242}Pu	4.4E–2
^{241}Am	1.497E–1

Table IB. Simulated Matrix and Matrix Density Combinations

Matrix (Number of densities)	Densities (g/cc)
Air (1)	0.001205
Metal (2)	0.03, 0.3
Salt (2)	0.07, 0.7
Polyethylene (26)	0.048-0.48 in steps of .024, 0.48-0.96 in steps of .048

7. SIMULATED DATA PROCESSING

The simulated data from MCNP6.2 simulations were processed in two ways:

1. Volume-average efficiency calculations
    a. Calculation of the simulated singles efficiency for the metal plutonium source at each of the fifteen positions for each combination of angle, matrix, and matrix density using all eighteen ^{3}He tubes.
    b. Calculation of the simulated volume-average singles efficiency for each combination of matrix and matrix density.
    c. Multiplicity analysis for each position using the F8 Pulse Height Tally data singles rate, doubles rate, and triples rate for all ^{3}He tubes, the volume-average efficiency, and the one sigma uncertainty of the volume-average efficiency.
2. PCE algorithm fitting and calculations
    a. Calibration of the PCE algorithm.
    b. Multiplicity analysis for each position using the F8 Pulse Height Tally data singles rate, doubles rate, and triples rate for all eighteen full-length ^{3}He tubes, the updated raw efficiency and raw one sigma uncertainty from the PCE algorithm. For direct comparison and to benefit analysis of the PCE algorithm, the singles, doubles, and triples from all eighteen full-length ^{3}He tubes are used. This represents a larger total active volume and, therefore, greater total efficiency than would be found with modified ^{3}He tube heights. This would change the detected singles, doubles, and triples rate for all assays equally, but would not change the difference between the assayed $^{240}Pu_{eff}$ using either a volume-average efficiency or the updated PCE algorithm efficiency and the declared $^{240}Pu_{eff}$.

8. RESULTS

The amount of data for comparison between multiplicity analysis using the volume-averaged efficiency and multiplicity using the updated PCE algorithm efficiency was large: fifteen positions per angle, for three angles, for each of the thirty-one combinations of matrix and matrix density, totaling 1,395 datapoints. Analysis showed that 1,205 cases were improved using the PCE algorithm, representing 86.4% of all datapoints.

8.1 Average Percent Difference

Since not all cases were improved, the average percent difference of the assayed $^{240}Pu_{eff}$ and declared $^{240}Pu_{eff}$ from multiplicity is a helpful metric for summarizing the average behavior of each method. When looking at the ninety-three combinations of angle, matrix, and matrix density, the average percent difference between assayed $^{240}Pu_{eff}$ and declared $^{240}Pu_{eff}$ was lower using the updated PCE algorithm efficiency for every combination. Figure 6 (left) compares the distributions of the average percent difference for all ninety-three combinations for the two methods. These results show a drastic decrease in the average percent difference of assayed $^{240}Pu_{eff}$ using the PCE algorithm. Figure 6 (right) shows the distribution of the reduction in average

percent difference using the updated PCE algorithm efficiency compared to the volume-average efficiency. Summary analysis of all ninety-three combinations showed that the PCE algorithm decreased the average percent difference by 67.2% on average.

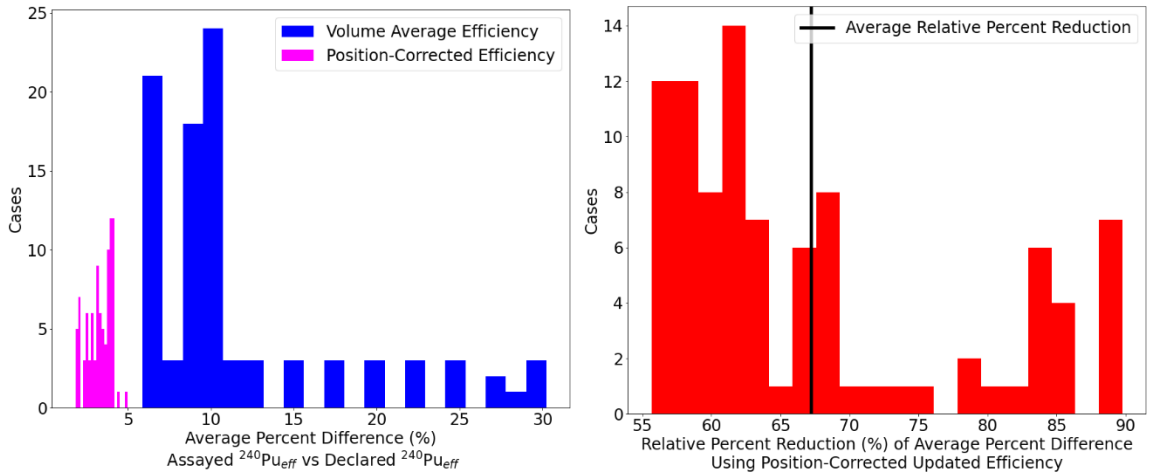

Figure 6. Results for the average percent difference between assayed $^{240}Pu_{eff}$ and declared $^{240}Pu_{eff}$. Left: Distributions of average percent difference for the two approaches. Right: Distribution of the relative reduction in average percent difference using the PCE algorithm.

8.2 Worst-Case Percent Difference

While the average percent difference is useful for understanding how the average case is impacted, waste assay is particularly interested in the worst-case percent difference as it represents the maximum assay deviation that can be encountered during assay. This value is used to determine the uncertainty contribution to instrument TMU. Thus, decreasing the worst-case percent difference drastically improves an instrument TMU. Comparing the two methods, when using the PCE algorithm the worst-case percent difference was again decreased for every combination. Figure 7 (left) compares the distributions of the worst-case percent difference for all ninety-three combinations for the two methods. These results show an extreme decrease in the worst-case percent difference. Figure 7 (right) shows the distribution of the reduction in worst-case percent difference using the updated PCE algorithm efficiency compared to the volume-average efficiency. Summary analysis of the ninety-three combinations showed that the PCE algorithm decreased the worst-case percent difference by 72.5% on average.

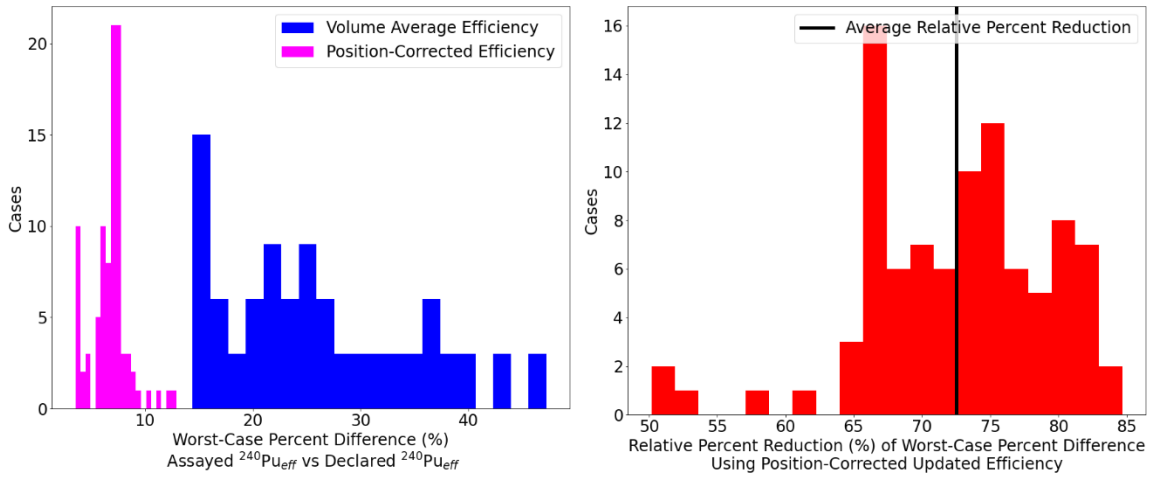

Figure 7. Results for the worst-case percent difference between assayed $^{240}Pu_{eff}$ and declared $^{240}Pu_{eff}$. Left: Distributions of worst-case percent difference for the two approaches. Right: Distribution of the relative reduction in worst-case percent difference using the PCE algorithm.

9. CONCLUSION

The PCE algorithm improves on all ninety-three combinations of angle, matrix, and matrix density tested for both the average percent difference and worst-case percent difference of the assayed $^{240}Pu_{eff}$ and declared $^{240}Pu_{eff}$. Further, the relative percent reduction for each metric is 67% or greater. These results from the MCNP6.2 simulation provide confidence that the PCE algorithm is a potentially useful algorithm for neutron NDA of waste materials from a nuclear facility. The PCE algorithm also underscores the benefits of list-mode data readouts and leverages them for a tangible outcome: decreased instrument TMU. These simulation results lay the groundwork for benchmarking the algorithm with measured data within a system like the HLNC-LM, which has full list-mode data readout capability but no axial resolution, and for designing a next-generation instrument with both radial and axial resolution. While the PCE algorithm demonstrates significant complexity and novelty, there are many exciting paths for further investigation and refinement of capabilities.

10. ACKNOWLEDGEMENT

This work was funded by NA-191 under the Dynamic Material Control (DYMAC) project. This work has been assigned LA-UR-23-24489.

11. REFERENCES

1. Reilly, D., Ensslin, N., & Smith, H. Jr. (1991). *Passive nondestructive assay of nuclear materials*. Nuclear Regulatory Commission and Office of Nuclear Regulatory Research. https://www.osti.gov/biblio/5428834
2. Langner, D. G., Stewart, J. E., Pickrell, M. M., Krick, M. S., Ensslin, N., & Harker, W. C. (1998). *Application Guide to Neutron Multiplicity Counting*. Los Alamos National Laboratory. https://www.osti.gov/biblio/1679
3. Menlove, H. O., Baca, J., Pecos, J. M., Davidson, D. R., McElroy, R. D., & Brochu, D. B. (1997). *HENC performance evaluation and plutonium calibration*. Los Alamos National Laboratory. https://www.osti.gov/biblio/564206
4. Menlove, H. O., Baca, J., Harker, W., Kroncke, K. E., Miller, M. C., Takahashi, S., Kobayashi, H., Seki, S., Matsuyama, K., & Kobayashi, S. (1992). *WDAS operation manual including the add-a-source function*. Los Alamos National Laboratory. https://www.osti.gov/biblio/10135451
5. *U.S. Department of Energy's Waste Isolation Pilot Plant - WIPP Site*. (n.d.). https://wipp.energy.gov/wipp-site.asp
6. Werner, C. J., Bull, J. S., Solomon, C J, Brown, F. B., McKinney, G. W., Rising, M. E., Dixon, D. A., Martz, R. L., Hughes, H. G., Cox, L. J., Zukaitis, A. J., Armstrong, J. C., Forster, R. A., & Casswell, L. (2018). *MCNP Version 6.2 Release Notes*. Los Alamos National Laboratory. https://www.osti.gov/biblio/1419730
7. Iliev, M., Ianakiev, K. D., & Swinhoe, M. T. (2016). *"KM200 Front-end Electronics for Thermal Neutron Detectors".* Proceedings of the 57th Annual Meeting of the Institute of Nuclear Materials Management (INMM 2016). http://toc.proceedings.com/32272webtoc.pdf
8. Newell, M. R., Rothrock, R., & Henzlova, D. (2017). *"Demonstration of the Advanced List Mode Module".* Proceedings of the 58th Annual Meeting of the Institute of Nuclear Materials Management (INMM 2017). http://toc.proceedings.com/38415webtoc.pdf
9. Nordquist, H. A., & Swinhoe, M. T. (2017). *INCC 6.0 - LANL's latest neutron coincidence counting software*. Los Alamos National Laboratory. https://www.osti.gov/biblio/1407860
10. Krick, M. S., & Menlove, H. O. (1979). *High-level neutron coincidence counter (HLNCC): users' manual*. Los Alamos National Laboratory. https://www.osti.gov/biblio/5830609